Soluble mannose receptor induces pro-inflammatory macrophage activation and obesity-associated metaflammation

Maria Embgenbroich[1,8], Hendrik J.P. van der Zande[2,8], Leonie Hussaarts[2,8], Jonas Schulte-Schrepping[3], Leonard R. Pelgrom[2], Noemí García-Tardón[2], Laura Schlautmann[1], Isabel Stoetzel[1], Kristian Händler[4], Joost M. Lambooij[2], Anna Zawistowska-Deniziak[2,7], Lisa Hoving[5], Karin de Ruiter[2], Marjolein Wijngaarden[6], Hanno Pijl[6], Ko Willems van Dijk[5,6], Bart Everts[2], Vanessa van Harmelen[5], Maria Yazdanbakhsh[2], Joachim L. Schultze[3,4], Bruno Guigas[2,9,*], Sven Burgdorf[1,9,*]

[1]Cellular Immunology, Life and Medical Sciences (LIMES) Institute, University of Bonn, Bonn, Germany

[2]Department of Parasitology, Leiden University Medical Center, Leiden, The Netherlands

[3]Genomics and Immunoregulation, Life and Medical Sciences (LIMES) Institute, University of Bonn, Bonn, Germany

[4]PRECISE Platform for Single Cell Genomics & Epigenomics, German Center for Neurodegenerative Diseases (DZNE) and University of Bonn, Bonn, Germany

[5]Department of Human Genetics, Leiden University Medical Center, Leiden, The Netherlands

[6]Department of Internal Medicine, Section Endocrinology Leiden University Medical Center Leiden The Netherlands

[7]Witold Stefański Institute of Parasitology, Polish Academy of Sciences, Warsaw, Poland

[8]These authors contributed equally

[9]These authors contributed equally

* Correspondence: Sven Burgdorf, Life and Medical Sciences (LIMES) Institute, Cellular Immunology, University of Bonn, Carl-Troll-Str. 31, 53115 Bonn, Germany; Tel. +49

2287362825; E-Mail: burgdorf@uni-bonn.de and Dr. Bruno Guigas, Department of Parasitology, Leiden University Medical Center, P.O. Box 9600, Postzone P4-P, 2300 RC Leiden, The Netherlands; Tel. +31 715261328; E-Mail: b.g.a.guigas@lumc.nl

Abstract

Pro-inflammatory activation of macrophages in metabolic tissues is critically important in induction of obesity-induced metaflammation. Here, we demonstrate that the soluble mannose receptor (sMR) plays a direct, functional role in both macrophage activation and metaflammation. We show that sMR binds CD45 on macrophages, both *in vitro* and *in vivo*, leading to cellular reprogramming towards an inflammatory phenotype by inhibition of CD45 phosphatase activity, which induces Src/Akt/NF-κB-mediated signaling. Remarkably, increased serum sMR levels were observed in obese mice and humans and directly correlated with body weight. Additionally, MR deficiency lowers the high-fat diet-induced increase in pro-inflammatory macrophages in metabolic tissues and protects against hepatic steatosis and whole-body metabolic dysfunctions. Conversely, administration of sMR in lean mice induces serum pro-inflammatory cytokines, activates tissue macrophages and promotes insulin resistance. Altogether, our results reveal sMR as novel regulator of pro-inflammatory macrophage activation and metaflammation, and could constitute a novel therapeutic target for hyperinflammatory diseases.

Introduction

Metaflammation defines a chronic inflammatory state in response to prolonged excessive nutrient intake and is characterized by low-grade inflammation of metabolic tissues [1]. Macrophage reprogramming towards an inflammatory phenotype plays a critical role in obesity-induced metaflammation [2]. In lean individuals, macrophages in metabolic tissues maintain tissue homeostasis and insulin sensitivity, potentially through secreting anti-inflammatory cytokines, e.g. TGFβ and IL-10 [1]. In metaflammation, however, macrophages in adipose tissue and liver are activated through pro-inflammatory factors in their microenvironment, such as high levels of saturated free fatty acids and IFN-γ. Consequently, these macrophages produce high amounts of tumor necrosis factor (TNF), which directly inhibits canonical insulin signaling [3], leading to ectopic fat deposition in the liver and in skeletal muscles [4]. Additionally, activation of Kupffer cells (KCs), the liver-resident macrophages, promotes recruitment and activation of inflammatory monocytes, which contribute to hepatic insulin resistance and steatosis [5,6].

Here, we describe a novel role of the mannose receptor (MR) on macrophage activation in the context of metaflammation. The MR (also termed CD206) is a type I transmembrane protein belonging to the C-type lectin family, which consists of a cysteine-rich region, a fibronectin type II domain, eight C-type lectin-like domains (CTLDs), a transmembrane region and a short cytosolic tail [7]. It is expressed by subpopulations of macrophages, dendritic cells and epithelial cells, with high expression levels in liver and lung [7,8]. Due to its high affinity for glycosylated antigens, the MR plays an important role in antigen uptake and presentation [9], and has an immune regulatory effect on other immune cells [10]. In addition to its functions as a transmembrane protein, the extracellular part of the MR can be shed by metalloproteases and released into the extracellular space [11,12]. Hence, soluble MR (sMR) can be detected in murine and human serum. Furthermore, increased serum levels of sMR have been detected in patients with a variety of inflammatory diseases, including pneumonia, liver cirrhosis, alcoholic liver

disease, gastric cancer, pneumococcal bacteremia, chronic hepatitis C, interstitial lung disease, sepsis and pulmonary tuberculosis [13–18]. Strikingly, in all these studies, sMR serum levels directly correlated with severity of disease and even with mortality. In addition, the sMR has been postulated as a biomarker for macrophage activation [13,16,18–20]. However, a physiological role of the sMR and a putative effect on macrophages have not been studied before. Therefore, it remains unclear whether increased serum levels of sMR in inflammatory diseases are merely a correlating phenomenon or whether the sMR actively triggers macrophage activation, contributing to the onset of inflammation.

Here, we report that sMR enhances macrophage activation, both *in vitro* and *in vivo*, and promotes metaflammation. We demonstrate that the sMR directly interacts with and inactivates the phosphatase CD45 on the surface of macrophages, leading to the activation of the Src/Akt/NF-κB pathway and cellular reprogramming towards an inflammatory phenotype. Additionally, we found enhanced sMR serum levels in HFD-induced obese mice and obese humans, and show that sMR-induced activation of macrophages *in vivo* impacts obesity-induced metaflammation and hepatic steatosis.

Results

Soluble MR enhances pro-inflammatory cytokine secretion by macrophages

To investigate whether the MR is involved in the pro-inflammatory activation of macrophages, we first stimulated bone marrow-derived macrophages from wild-type or MR-deficient mice with LPS. We found increased secretion of the pro-inflammatory cytokines TNF and IL-6 in MR-expressing wild-type macrophages (Figure 1a). This could be explained by two possibilities. First, the MR at the cell membrane might bind extracellular ligands and pass on an activating signal in macrophages. However, no MR-mediated signaling has been reported so far. Second, since the extracellular region of the MR is shed by metalloproteases and released into the extracellular space as a soluble protein (sMR) (Supplementary Figure 1), the observed effects might also be induced by direct binding of the sMR to interacting proteins on the cell surface of the macrophages. To distinguish between these two scenarios, we generated a fusion protein between the Fc region of human IgG1 and the extracellular region of the MR (encompassing the cysteine-rich region, the fibronectin region and CTLD1-2) (FcMR) [10]. Treatment of MR-deficient macrophages with FcMR enhanced secretion of TNF and IL-6 after LPS stimulation compared to isotype control-treated cells (Figure 1b), suggesting that binding of sMR to the macrophage surface might be responsible for the observed effect. We observed similar results when treating MR-deficient macrophages with commercially available recombinant MR protein, consisting of the complete extracellular region of the protein (Figure 1c). To definitively prove that sMR is responsible for the increase in cytokine production, we purified sMR from the supernatant of MR-expressing macrophages (Supplementary Figure 1). Treating MR-deficient macrophages with purified sMR indeed increased the secretion of TNF after LPS stimulation (Supplementary Figure 1). Similar results were obtained from FcMR-treated primary macrophages isolated from murine liver, spleen or peritoneal cavity (PEC) (Figure 1d), and from human monocyte-derived macrophages after addition of recombinant

human MR (Figure 1e) or siRNA-mediated down-regulation of the MR (Figure 1f), demonstrating that the sMR alters the cytokine profile of a broad range of macrophages.

sMR induces a pro-inflammatory phenotype in macrophages

To further dissect the effect of the sMR on macrophages, we treated MR-deficient macrophages with FcMR for 4 h, 12 h or 24 h and performed RNA-seq analysis (Figure 2a). Principle component analysis (PCA) based on variance-stabilized counts of all 23,250 present genes revealed clear transcriptomic distinction of the samples of all analyzed conditions both due to FcMR treatment and time (Figure 2b). A heatmap of the union of the 1366 differentially expressed (DE) genes between FcMR treatment and control presented the substantial changes in gene expression due to the FcMR treatment over time with overlapping and unique gene sets (Figure 2c, Supplementary figure 2). Gene ontology enrichment analysis (GOEA) based on these shared and specific DE gene sets upregulated upon FcMR treatment clearly demonstrated inflammatory activation of macrophages (Supplementary Figure 2). The most significantly upregulated genes in response to FcMR treatment further emphasized the strong and dynamic inflammatory activation of macrophages, with well-known immunological key mediators such as TNF, IL-6 and IL12, exhibiting very specific expression patterns (Figure 2d). To classify the response elicited by sMR within the broad spectrum of macrophage activation phenotypes, we performed an enrichment analysis using macrophage activation signatures derived from our previous study comprising macrophages treated with 28 different immunological stimuli [21] and the gene sets of FcMR-mediated up-regulated genes per time point. This analysis revealed a striking similarity of FcMR-induced expression patterns to macrophage signatures associated with a chronic inflammatory phenotype, as induced by TNF, PGE2, and P3C (TPP) in our previous stimulation study (Figure 2e, Supplementary Figure 2), further substantiating that the sMR reprograms macrophages towards a pro-inflammatory phenotype.

sMR activates macrophages by binding and inhibiting CD45

Next, we investigated the molecular mechanisms regulating sMR-induced macrophage reprogramming and searched for binding partners of sMR on the macrophage surface. To this end, we isolated cell lysates from macrophages that previously underwent surface biotinylation, and performed immunoprecipitation using FcMR. Western Blot analysis using streptavidin allowed us to monitor cell surface proteins interacting with sMR, including a clear band at the molecular weight of the phosphatase CD45 (between 180 and 220 kDa, depending on the splice variant) (Supplementary Figure 3), a known binding partner of the MR [22]. Indeed, co-immunoprecipitation experiments revealed an interaction of the sMR with CD45 on macrophages (Figures 3a, 3b).

CD45 can be expressed as different isoforms, depending on the alternative splicing of its three exons A, B and C. To identify the isoform interacting with sMR, we assessed the expression of CD45 isoforms using isoform-specific antibodies. Analysis by Western Blot and flow cytometry clearly showed the absence of exons A, B and C in bone marrow-derived macrophages (Supplementary Figure 3), pointing out that these cells only express the CD45RO isoform and hence, the MR interacts with CD45RO. This is in accordance with our RNA-seq data, which showed a specific read coverage of all exons of *Cd45* except for exons A, B and C (Supplementary Figure 3). Additionally, we analyzed the CD45 isotypes on primary macrophages from spleen, white adipose tissue (WAT), liver and the peritoneal cavity. Macrophages from these tissues also expressed the CD45RO isoform (Supplementary Figure 3), which is in agreement with previous literature [23]. Accordingly, we confirmed the direct interaction of FcMR with CD45RO from primary splenic macrophages by far Western Blot (Supplementary Figure 3).

Since little is known about CD45 phosphatase activity in macrophages, we next investigated whether CD45 is active in these cells. Therefore, we immunoprecipitated CD45 from macrophage lysates and added 4-nitrophenyl phosphate (pNPP), from which dephosphorylation by CD45 can be quantified using colorimetry. We monitored a clear phosphatase activity, which was blocked by a CD45-specific inhibitor (Supplementary Figure 3), demonstrating the presence of active CD45 in macrophages. Next, we tested the effect of sMR on CD45 phosphatase activity. To this end, we precipitated CD45 from macrophage lysates that were pre-treated with FcMR. Dephosphorylation of pNPP was inhibited in the presence of FcMR (Figure 3c), indicating that sMR may inhibit the phosphatase activity of CD45. In a second approach, we tested the dephosphorylation of a synthetic peptide containing pY505 of Lck, a specific substrate of CD45, using a phospho-specific antibody. Here, pre-incubation with FcMR increased pY505 phosphorylation (Figure 3d), confirming an inhibitory effect of sMR on the phosphatase activity of CD45.

To investigate whether sMR-mediated inhibition of CD45 phosphatase activity plays a role in macrophage activation, we down-regulated CD45 expression using siRNA (Supplementary Figure 3). Similar to inhibition of CD45 by sMR, CD45 down-regulation resulted in increased expression of TNF and IL-6 after stimulation with LPS (Figure 3e). Importantly, addition of FcMR after CD45 down-regulation had no further effect on cytokine secretion (Figure 3f), demonstrating that the activating effect of the MR on macrophages was indeed due to its inhibition of CD45.

sMR-mediated inhibition of CD45 activates a Src/Akt/NF-κB signaling cascade in macrophages

We next investigated how sMR-mediated inhibition of CD45 results in macrophage reprogramming towards a pro-inflammatory phenotype. First, we screened for over-represented transcription factor (TF) binding motifs in the non-protein coding regions of FcMR-specific upregulated DE genes. Network visualization of enriched TF binding motifs and their potential target DE genes clearly exposed NF-κB as the dominating transcriptional regulator of differential gene expression across all three time points (Figure 4a). Indeed, macrophage treatment with FcMR significantly downregulated IκBα (Figure 4b), an inhibitor of NF-κB that disables nuclear translocation of NF-κB, retaining NF-κB in the cytosol. Accordingly, enhanced nuclear translocation of both NF-κB subunits p65 and p50 was observed after FcMR treatment (Figure 4c).

Subsequently, we identified the signaling cascade leading from FcMR-mediated inhibition of CD45 to activation of NF-κB. Previous studies have shown that activation of Src kinases, which are a direct substrate of CD45 and become inactivated upon CD45-mediated dephosphorylation [24], leads to degradation of IκBα and activation of NF-κB [25–27]. Additionally, CD45 prevents Akt signaling [28,29], which is directly activated by Src [30], resulting in IKK-mediated degradation of IκBα and activation of NF-κB [31,32]. Therefore, we investigated whether FcMR-mediated inhibition of CD45 results in NF-κB activation through signaling via Src and Akt. Indeed, FcMR treatment increased phosphorylation, and hence activation, of Src (Figure 4d). Furthermore, blocking Src using three different chemical inhibitors (PP2, KX2-391 and A419259) markedly decreased TNF secretion (Figure 4e). Of note, the effect of FcMR on TNF secretion was completely abolished in the presence of these Src inhibitors (Figure 4f), demonstrating that FcMR-induced macrophage activation depends on Src signaling. Similarly, FcMR treatment clearly increased phosphorylation of Akt (Figure 4g) and addition of an Akt-specific inhibitor decreased LPS-induced secretion of TNF and IL-6 (Figure 4h). Also here, in the presence of the Akt inhibitor, the stimulatory effect of FcMR on TNF secretion was

abolished (Figure 4i), showing an important role for Akt signaling in FcMR-enhanced TNF secretion. Accordingly, inhibition of Akt prevented FcMR-induced translocation of NF-κB into the nucleus (Supplementary Figure 4), confirming that macrophage activation and nuclear translocation of NF-κB via the FcMR depend on Akt signaling.

Taken together, these data unequivocally show that sMR-mediated inhibition of CD45 results in activation of Src/Akt signaling leading to nuclear translocation of NF-κB and macrophage reprogramming towards an inflammatory phenotype.

Serum sMR is up-regulated in obesity and promotes HFD-induced metabolic dysfunctions and hepatic steatosis

Next, we monitored whether the inflammatory effect of the MR on macrophages regulates inflammatory processes *in vivo* using a murine model of obesity-induced metaflammation. Therefore, we first analyzed putative changes in MR expressing cells as sources for sMR after feeding mice a high fat diet (HFD). In spleen and white adipose tissue (WAT), nearly all MR-expressing cells were $CD45^+$, whereas in liver, $CD45^-$ cells also expressed the MR. These latter cells were identified as $CD31^+CD146^+$ liver sinusoidal endothelial cells (LSECs), which were indeed previously reported to express the MR [7]. Importantly, whereas no differences in MR expression could be detected in $CD45^-$ cells, a clear increase in MR^+ cells was observed in $CD45^+$ hematopoietic cells in spleen, liver and WAT of HFD-fed obese mice compared to control diet (CD)-fed mice (Figure 5a). Of note, $CD45^+MR^+$ cells in all three organs were mainly identified as $CD64^+F4/80^+$ macrophages (Supplementary Figure 5). Taken together, this demonstrates that obesity increased MR-expressing macrophages in spleen, liver and WAT.

We next investigated whether HFD feeding also resulted in elevated serum sMR levels (Supplementary Figure 5) and we demonstrated significantly increased sMR concentrations in the serum of HFD-fed obese mice, as compared to lean CD-fed mice (Figure 5b). Additionally,

serum sMR levels positively correlated with body weight and fat mass of the mice (Figures 5c, 5d). In humans, serum sMR levels were also increased in obese individuals when compared to lean subjects (Figure 5e), and correlated positively with body mass index (BMI) and fat mass (Figures 5f, 5g), indicating a direct correlation between serum sMR levels and obesity in both humans and mice.

To test whether the MR regulates macrophage-mediated inflammatory diseases *in vivo*, we then analyzed the development of obesity-induced metaflammation in MR-deficient mice. Whereas no differences in body weights were found between wild-type and MR-deficient mice on CD, MR-deficient mice were partially protected from weight gain on a HFD (Figure 5h). Analysis of body composition showed that the lower body weight in HFD-fed MR-deficient mice resulted exclusively from a reduction in fat mass, without affecting lean mass (Figure 5i). Accordingly, the weights of epididymal, mesenteric and subcutaneous (inguinal) WAT, as well as brown adipose tissue (BAT), were significantly lower in MR-deficient mice on HFD (Supplementary Figure 5). In addition, liver weight was also markedly lower in HFD-fed MR-deficient mice as compared to wild-type controls (Figure 5j), suggesting a reduction in hepatic steatosis. Indeed, MR-deficient mice were completely protected against HFD-induced hepatic steatosis (Figure 5k). Accordingly, hepatic triglycerides, total cholesterol and phospholipids contents (Supplementary Figure 5) and circulating alanine aminotransaminase (ALAT) levels (Supplementary Figure 5) were markedly decreased in HFD-fed MR-deficient mice.

HFD-fed MR-deficient mice displayed significantly lower fasting plasma insulin levels than wild-type mice, whereas fasting glucose levels were unchanged (Supplementary Figure 5). The calculated HOmeostasis Model Assessment of Insulin Resistance index (HOMA-IR) adjusted for mice was significantly reduced in HFD-fed MR-deficient mice (Supplementary Figure 5), suggesting that insulin resistance is less severe in these mice. In line with this, whole-body insulin sensitivity (Figure 5l) and glucose tolerance (Figure 5m) were significantly higher in HFD-fed MR-deficient mice compared to wild-type mice. Of note, the alleviated hepatic

steatosis and whole-body metabolic homeostasis were still observed when HFD-fed MR-deficient mice were weight-paired to their wild-type counterparts (Supplementary Figure 5), indicating that MR deficiency protects against HFD-induced metabolic dysfunctions independently of body weight changes. Altogether, these data demonstrate that MR expression contributes to obesity-induced metabolic dysfunctions.

MR promotes inflammatory macrophage accumulation in eWAT and liver during obesity

Since our *in vitro* data clearly demonstrate that the MR reprograms macrophages towards an inflammatory phenotype, we next investigated whether MR deficiency protects against pro-inflammatory macrophage accumulation in metabolic tissues of obese mice.

As previously reported, HFD significantly increased obesity-associated pro-inflammatory $CD11c^+$ adipose tissue macrophages (ATMs) in eWAT of wild-type mice [33], whereas total ATMs and $CD11b^+Ly6C^+$ monocytes were not affected (Figure 6a, Supplementary Figure 6). Remarkably, while no significant differences in total ATMs and monocyte numbers were observed between genotypes, inflammatory $CD11c^+$ ATM numbers were found to be significantly higher in HFD-fed MR-expressing wild-type mice as compared to MR-deficient mice (Figure 6a).

In the liver, HFD significantly increased pro-inflammatory $CD11c^+$ KCs and $CD11b^+Ly6C^+$ monocytes in wild-type mice, while total KCs were not affected (Figure 6b). Similar to what was observed in eWAT, inflammatory $CD11c^+$ KCs, but also monocytes, were more abundant in liver of MR-expressing wild-type mice as compared to MR-deficient mice, while total KCs were not affected (Figure 6b). This was associated with higher expression of genes involved in pro-inflammatory macrophage activation in liver and WAT of MR-expressing wild-type mice (Supplementary Figure 6). The differences in pro-inflammatory macrophage abundances in metabolic tissues were still present when wild-type and MR-deficient mice were weight-paired

(Supplementary Figure 6), demonstrating that also the regulation of obesity-induced pro-inflammatory macrophages by the MR is independent of changes in body weight. Additionally, a strong positive correlation between the numbers of pro-inflammatory macrophages in eWAT and liver, and whole-body insulin resistance was observed (Figures 6c, 6d).

sMR treatment induces pro-inflammatory cytokines, metabolic dysfunctions and increased pro-inflammatory macrophages

Finally, we investigated whether *in vivo* administration of FcMR also induces macrophage activation and metabolic dysfunctions. Therefore, we first monitored circulating cytokine levels in response to a single intraperitoneal injection of FcMR in CD-fed lean mice. In accordance with our *in vitro* experiments, injection of FcMR acutely increased serum levels of TNF and IL-6 and of the chemokine MCP-1/CCL2 compared to isotype control-treated mice (Figure 7a). To assess whether increased sMR levels also promote whole-body metabolic dysfunctions, we injected lean mice with FcMR or isotype control every three days. After four weeks of treatment, we monitored a mild increase in body weight in FcMR-treated mice compared to control mice (Figures 7b, 7c). In addition, insulin sensitivity, as measured by an acute drop in blood glucose levels following insulin i.p. injection, was reduced in FcMR-treated mice compared to control mice (Figures 7d, 7e), confirming the regulatory effect of the sMR on whole-body metabolism. Of note, when mice were fed a HFD concomitantly with four weeks FcMR treatment, the effect of FcMR on HFD-induced insulin resistance was even amplified (Supplementary Figure 7).

FcMR treatment increased macrophage numbers in eWAT of lean mice (Figure 7f). Moreover, gene expression of *Il1b, Tnf, Il6* and *Ccl2* was increased in eWAT of FcMR-treated lean mice (Figure 7g). Accordingly, macrophages isolated from these mice showed increased secretion of most of these cytokines upon stimulation with LPS (Figure 7h), demonstrating that, in lean

mice, increased serum sMR levels induce macrophage reprogramming towards an inflammatory phenotype in metabolic tissues.

Taken together, these data show that increased sMR levels induce the secretion of pro-inflammatory cytokines, induce whole-body insulin resistance and promote macrophage activation in metabolic tissues *in vivo*.

Discussion

The MR as a member of the C-type lectin family has mainly been described as an endocytic receptor recognizing glycosylated antigens and mediating antigen processing and presentation [34]. However, the extracellular region of the MR (sMR) can be shed by metalloproteases and released as a soluble protein in the extracellular space. Consequently, the sMR is detectable in murine and human serum [11,12], and recent studies reported an increase of serum sMR levels in a variety of inflammatory diseases. Serum sMR levels directly correlated with severity of disease and mortality [13–18] and the sMR has been postulated as biomarker for macrophage-mediated inflammatory diseases [13,16,18–20]. However, these studies merely monitored phenotypic correlations. Here, we demonstrated that the sMR plays a direct, functional role in macrophage activation, driving reprogramming towards a pro-inflammatory phenotype. By interacting with and inactivating CD45, the sMR reprograms macrophages via activation of Src/Akt signaling and nuclear translocation of NF-κB. *In vivo*, sMR levels were increased in obese mice and humans as compared to lean controls, and we found that MR deficiency protects against obesity-induced metabolic dysfunctions, which correlated strongly with decreased HFD-induced inflammatory macrophages in adipose tissue and liver. Consistently, injection of FcMR acutely increased pro-inflammatory cytokines in the circulation, and induced macrophage activation and insulin resistance in metabolic tissues also in lean mice. It is hence conceivable that increased sMR levels might also play a causal role in the development of other inflammatory diseases associated with increased serum sMR levels.

In this study, we found increased MR^+ cells in spleen, liver and eWAT upon HFD feeding, which were almost exclusively macrophages. Since it has been demonstrated that cell surface MR is shed by serum proteases and released as a soluble form, obesity-induced changes in tissue homeostasis may increase MR expression and sMR release by macrophages, creating increased local and systemic sMR levels to promote macrophage-mediated inflammation and

whole-body metabolic dysfunctions. An important factor in this process could be the ligand-inducible transcription factor PPARγ, which is activated, among others, by free fatty acids. Indeed, single cell RNA sequencing analysis of adipose tissue immune cells revealed that PPAR signaling is among the upregulated pathways in obesity-induced lipid-associated macrophages (LAMs) in both mice and humans [35]. Since *Mrc1* (encoding the MR) is also a direct target gene of PPARγ [36], obesity-induced activation of PPARγ in macrophages may lead to enhanced transcription of the MR, eventually resulting in increased sMR levels.

Our data clearly demonstrate that macrophage activation by the MR was due to MR-mediated inhibition of CD45, which in turn leads to activation of Src and Akt, and nuclear translocation of NF-κB. Src kinases have been demonstrated manifold to be direct substrates of CD45 and CD45-mediated dephosphorylation of Src leads to its inactivation [24]. Activation of Src leads to activation of Akt [30], which in turn promotes nuclear translocation of NF-κB [25–27]. Of note, it has been reported that activation of Src kinases can lead to activation of NF-κB independent of Akt. Such signaling has been demonstrated to be mediated by the Bruton's tyrosine kinase (BTK) [37,38]. Here, MR-induced macrophage activation was not affected by BTK, as inhibition of BTK by Ibrutinib did not influence secretion of TNF and IL-6 by macrophages (data not shown). In contrast, MR-mediated macrophage activation depended on Akt signaling, as Akt inhibition abrogated MR-mediated nuclear translocation of NF-κB and ensuing TNF and IL-6 secretion by macrophages. It has been demonstrated before that Akt plays an important role in regulating efficient binding of p65 to specific target promoters. Therefore, Akt has been postulated as a regulator that can fine tune NF-κB-mediated responses [32]. Of note, these authors demonstrated that NF-κB-mediated expression of TNF was particularly sensitive to Akt signaling, which is in accordance with the Akt-dependency of TNF expression after MR-induced activation of macrophages described here.

The immunometabolic phenotype of obese MR-deficient mice resembles that of mice deficient for MGL/CLEC10A, another member of the C-type lectin family. Indeed, these mice displayed reduced hepatic steatosis, insulin resistance and glucose intolerance upon HFD when compared to wild-type mice, a feature that was associated with lower AT pro-inflammatory macrophages [39]. In another context, MGL/CLEC10A was also shown to bind and inactivate CD45 [40], offering the possibility that MGL/CLEC10A can directly induce macrophage reprogramming by inhibition of CD45, similar to the MR. Future studies will have to reveal whether MGL/CLEC10A indeed plays a direct role in macrophage activation, whether its expression is also increased in HFD-induced obesity, and whether this may be mediated by a soluble form of MGL/CLEC10A.

MR-mediated inhibition of CD45 and concomitant activation of macrophages might open possibilities for therapeutics aimed at dampening inflammation. Given the important role of the MR in HFD-induced metabolic dysfunctions, antibodies, nanobodies, aptamers or small molecules that prevent MR binding to CD45 could block disease progression.

In summary, we demonstrate that a soluble form of the MR reprograms macrophages towards an inflammatory phenotype by interacting with CD45 on the surface of these macrophages. MR-mediated inhibition of CD45 activated Src and Akt kinases, resulting in nuclear translocation of NF-κB and inflammatory cytokine production. Furthermore, sMR levels in serum of obese mice and humans are increased, strongly correlating to metabolic dysfunctions. Accordingly, deficiency in MR resulted in fewer HFD-induced pro-inflammatory macrophages in WAT and liver, and protection from metaflammation and hepatic steatosis, whereas increased MR serum levels induced pro-inflammatory cytokines in circulation, macrophage activation and exacerbated whole-body metabolic dysfunctions. These data identify the MR as novel regulator of metaflammation and contribute to a better understanding of macrophage-mediated inflammatory diseases.

Acknowledgements

This work is funded by the Deutsche Forschungsgemeinschaft (DFG, German Research Foundation) under Germany´s Excellence Strategy – EXC2151 – 390873048 (to SB), an EFSD/Lilly Research Grant Fellowship from the European Federation for the Study of Diabetes (to BG), the NWO Graduate School Program 022.006.010 (to HJPvdZ), and the Dutch Organization for Scientific Research (ZonMW TOP Grant 91214131, to BG and MY). We thank Frank Otto and Arifa Ozir-Fazalalikhan for their precious technical help.

Author contributions

Conceptualization: B.G. and S.B.; Methodology: B.G., S.B., J.L.S., M.E., H.J.P.vdZ, L.H., K.H., J.S.-S., V.vH, B.E.; Investigation: B.G., S.B., M.E., H.J.P.vdZ, L.H., J.S.-S., L.S., I.S., N.G-T, J.L., A.Z, L.H., K.dR, M.W, V.vH, L.R.P., B.E.; Writing – Original Draft: B.G, S.B., H.J.P.vdZ, M.E, J. S.-S., J.L.S.; Writing – Review & Editing, ; Funding Acquisition:, S.B., B.G, J.L.S., M.Y., H.J.P.vdZ; Resources: M.W, H.P., K.WvD; Supervision: S.B. B.G., J.L.S., K.H., M.Y., V.vH, K.WvD, B.E.

The authors declare no competing interests.

References

1. Brestoff, J. R. & Artis, D. Immune regulation of metabolic homeostasis in health and disease. *Cell* **161,** 146–160; 10.1016/j.cell.2015.02.022 (2015).

2. Hotamisligil, G. S. Inflammation, metaflammation and immunometabolic disorders. *Nature* **542,** 177–185; 10.1038/nature21363 (2017).

3. Hotamisligil, G. S., Murray, D. L., Choy, L. N. & Spiegelman, B. M. Tumor necrosis factor alpha inhibits signaling from the insulin receptor. *Proceedings of the National Academy of Sciences of the United States of America* **91,** 4854–4858; 10.1073/pnas.91.11.4854 (1994).

4. Shulman, G. I. Ectopic fat in insulin resistance, dyslipidemia, and cardiometabolic disease. *The New England journal of medicine* **371,** 2237–2238; 10.1056/NEJMc1412427 (2014).

5. Neuschwander-Tetri, B. A. Hepatic lipotoxicity and the pathogenesis of nonalcoholic steatohepatitis: the central role of nontriglyceride fatty acid metabolites. *Hepatology (Baltimore, Md.)* **52,** 774–788; 10.1002/hep.23719 (2010).

6. Lanthier, N. *et al.* Kupffer cell activation is a causal factor for hepatic insulin resistance. *American journal of physiology. Gastrointestinal and liver physiology* **298,** G107-16; 10.1152/ajpgi.00391.2009 (2010).

7. Martinez-Pomares, L. The mannose receptor. *Journal of leukocyte biology* **92,** 1177–1186; 10.1189/jlb.0512231 (2012).

8. Takahashi, K., Donovan, M. J., Rogers, R. A. & Ezekowitz, R. A. Distribution of murine mannose receptor expression from early embryogenesis through to adulthood. *Cell and tissue research* **292,** 311–323; 10.1007/s004410051062 (1998).

9. Burgdorf, S., Kautz, A., Böhnert, V., Knolle, P. A. & Kurts, C. Distinct pathways of antigen uptake and intracellular routing in CD4 and CD8 T cell activation. *Science (New York, N.Y.)* **316,** 612–616; 10.1126/science.1137971 (2007).

10. Schuette, V. *et al.* Mannose receptor induces T-cell tolerance via inhibition of CD45 and up-regulation of CTLA-4. *Proceedings of the National Academy of Sciences of the United States of America* **113,** 10649–10654; 10.1073/pnas.1605885113 (2016).

11. Jordens, R., Thompson, A., Amons, R. & Koning, F. Human dendritic cells shed a functional, soluble form of the mannose receptor. *International immunology* **11,** 1775–1780; 10.1093/intimm/11.11.1775 (1999).

12. Martínez-Pomares, L. *et al.* A functional soluble form of the murine mannose receptor is produced by macrophages in vitro and is present in mouse serum. *The Journal of biological chemistry* **273,** 23376–23380; 10.1074/jbc.273.36.23376 (1998).

13. Saha, B. *et al.* Biomarkers of Macrophage Activation and Immune Danger Signals Predict Clinical Outcomes in Alcoholic Hepatitis. *Hepatology (Baltimore, Md.)* **70,** 1134–1149; 10.1002/hep.30617 (2019).

14. Suzuki, Y. *et al.* Macrophage mannose receptor, CD206, predict prognosis in patients with pulmonary tuberculosis. *Scientific reports* **8,** 13129; 10.1038/s41598-018-31565-5 (2018).

15. Rødgaard-Hansen, S. *et al.* Increased concentrations of the soluble mannose receptor in serum from patients with pneumococcal bacteraemia, and prediction of survival. *Infectious diseases (London, England)* **47,** 203–208; 10.3109/00365548.2014.984321 (2015).

16. Ding, D., Song, Y., Yao, Y. & Zhang, S. Preoperative serum macrophage activated biomarkers soluble mannose receptor (sMR) and soluble haemoglobin scavenger receptor (sCD163), as novel markers for the diagnosis and prognosis of gastric cancer. *Oncology letters* **14,** 2982–2990; 10.3892/ol.2017.6547 (2017).

17. Loonen, A. J. M. *et al.* Soluble mannose receptor levels in blood correlate to disease severity in patients with community-acquired pneumonia. *Immunology letters* **206,** 28–32; 10.1016/j.imlet.2018.12.001 (2019).

18. Andersen, E. S. *et al.* Macrophage-related serum biomarkers soluble CD163 (sCD163) and soluble mannose receptor (sMR) to differentiate mild liver fibrosis from cirrhosis in patients with chronic hepatitis C: a pilot study. *European journal of clinical microbiology & infectious diseases : official publication of the European Society of Clinical Microbiology* **33,** 117–122; 10.1007/s10096-013-1936-3 (2014).

19. Andersen, M. N. *et al.* Soluble Macrophage Mannose Receptor (sCD206/sMR) as a Biomarker in Human Immunodeficiency Virus Infection. *The Journal of infectious diseases* **218,** 1291–1295; 10.1093/infdis/jiy318 (2018).

20. Fan, W. *et al.* Identification of CD206 as a potential biomarker of cancer stem-like cells and therapeutic agent in liver cancer. *Oncology letters* **18,** 3218–3226; 10.3892/ol.2019.10673 (2019).

21. Xue, J. *et al.* Transcriptome-based network analysis reveals a spectrum model of human macrophage activation. *Immunity* **40,** 274–288; 10.1016/j.immuni.2014.01.006 (2014).

22. Martínez-Pomares, L. *et al.* Cell-specific glycoforms of sialoadhesin and CD45 are counter-receptors for the cysteine-rich domain of the mannose receptor. *The Journal of biological chemistry* **274,** 35211–35218; 10.1074/jbc.274.49.35211 (1999).

23. Pilling, D., Fan, T., Huang, D., Kaul, B. & Gomer, R. H. Identification of markers that distinguish monocyte-derived fibrocytes from monocytes, macrophages, and fibroblasts. *PloS one* **4,** e7475; 10.1371/journal.pone.0007475 (2009).

24. Shrivastava, P., Katagiri, T., Ogimoto, M., Mizuno, K. & Yakura, H. Dynamic regulation of Src-family kinases by CD45 in B cells. *Blood* **103,** 1425–1432; 10.1182/blood-2003-03-0716 (2004).

25. Xie, X. *et al.* Connexin43 mediates NF-κB signalling activation induced by high glucose in GMCs: involvement of c-Src. *Cell communication and signaling : CCS* **11,** 38; 10.1186/1478-811X-11-38 (2013).

26. Lluis, J. M., Buricchi, F., Chiarugi, P., Morales, A. & Fernandez-Checa, J. C. Dual role of mitochondrial reactive oxygen species in hypoxia signaling: activation of nuclear factor-{kappa}B via c-SRC and oxidant-dependent cell death. *Cancer research* **67,** 7368–7377; 10.1158/0008-5472.CAN-07-0515 (2007).

27. Abu-Amer, Y. *et al.* Tumor necrosis factor-alpha activation of nuclear transcription factor-kappaB in marrow macrophages is mediated by c-Src tyrosine phosphorylation of Ikappa Balpha. *The Journal of biological chemistry* **273,** 29417–29423; 10.1074/jbc.273.45.29417 (1998).

28. Suh, H.-S., Kim, M.-O. & Lee, S. C. Inhibition of granulocyte-macrophage colony-stimulating factor signaling and microglial proliferation by anti-CD45RO: role of Hck tyrosine kinase and phosphatidylinositol 3-kinase/Akt. *Journal of immunology (Baltimore, Md. : 1950)* **174,** 2712–2719; 10.4049/jimmunol.174.5.2712 (2005).

29. Zhu, J. W. *et al.* Receptor-like tyrosine phosphatases CD45 and CD148 have distinct functions in chemoattractant-mediated neutrophil migration and response to S. aureus. *Immunity* **35,** 757–769; 10.1016/j.immuni.2011.09.011 (2011).

30. Chen, J. The Src/PI3K/Akt signal pathway may play a key role in decreased drug efficacy in obesity-associated cancer. *Journal of cellular biochemistry* **110,** 279–280; 10.1002/jcb.22572 (2010).

31. Bai, D., Ueno, L. & Vogt, P. K. Akt-mediated regulation of NFkappaB and the essentialness of NFkappaB for the oncogenicity of PI3K and Akt. *International journal of cancer* **125,** 2863–2870; 10.1002/ijc.24748 (2009).

32. Cheng, J., Phong, B., Wilson, D. C., Hirsch, R. & Kane, L. P. Akt fine-tunes NF-κB-dependent gene expression during T cell activation. *The Journal of biological chemistry* **286,** 36076–36085; 10.1074/jbc.M111.259549 (2011).

33. Lumeng, C. N., Bodzin, J. L. & Saltiel, A. R. Obesity induces a phenotypic switch in adipose tissue macrophage polarization. *The Journal of clinical investigation* **117,** 175–184; 10.1172/JCI29881 (2007).

34. Kreer, C. *et al.* N-glycosylation converts non-glycoproteins into mannose receptor ligands and reveals antigen-specific T cell responses in vivo. *Oncotarget* **8,** 6857–6872; 10.18632/oncotarget.14314 (2017).

35. Jaitin, D. A. *et al.* Lipid-Associated Macrophages Control Metabolic Homeostasis in a Trem2-Dependent Manner. *Cell* **178,** 686-698.e14; 10.1016/j.cell.2019.05.054 (2019).

36. Klotz, L. *et al.* Increased antigen cross-presentation but impaired cross-priming after activation of peroxisome proliferator-activated receptor gamma is mediated by up-regulation of B7H1. *Journal of immunology (Baltimore, Md. : 1950)* **183,** 129–136; 10.4049/jimmunol.0804260 (2009).

37. Doyle, S. L., Jefferies, C. A. & O'Neill, L. A. Bruton's tyrosine kinase is involved in p65-mediated transactivation and phosphorylation of p65 on serine 536 during NFkappaB activation by lipopolysaccharide. *The Journal of biological chemistry* **280,** 23496–23501; 10.1074/jbc.C500053200 (2005).

38. Weber, A. N. R. *et al.* Bruton's Tyrosine Kinase: An Emerging Key Player in Innate Immunity. *Frontiers in immunology* **8,** 1454; 10.3389/fimmu.2017.01454 (2017).

39. Westcott, D. J. *et al.* MGL1 promotes adipose tissue inflammation and insulin resistance by regulating 7/4hi monocytes in obesity. *The Journal of experimental medicine* **206,** 3143–3156; 10.1084/jem.20091333 (2009).

40. van Vliet, S. J., Gringhuis, S. I., Geijtenbeek, T. B. H. & van Kooyk, Y. Regulation of effector T cells by antigen-presenting cells via interaction of the C-type lectin MGL with CD45. *Nature immunology* **7,** 1200–1208; 10.1038/ni1390 (2006).

41. Wijngaarden, M. A., van der Zon, G. C., van Dijk, K. W., Pijl, H. & Guigas, B. Effects of prolonged fasting on AMPK signaling, gene expression, and mitochondrial respiratory chain content in skeletal muscle from lean and obese individuals. *American journal of physiology. Endocrinology and metabolism* **304,** E1012-21; 10.1152/ajpendo.00008.2013 (2013).

42. Hussaarts, L. *et al.* Rapamycin and omega-1: mTOR-dependent and -independent Th2 skewing by human dendritic cells. *Immunology and cell biology* **91,** 486–489; 10.1038/icb.2013.31 (2013).

43. Soneson, C., Love, M. I. & Robinson, M. D. Differential analyses for RNA-seq: transcript-level estimates improve gene-level inferences. *F1000Research* **4,** 1521; 10.12688/f1000research.7563.2 (2015).

44. Love, M. I., Huber, W. & Anders, S. Moderated estimation of fold change and dispersion for RNA-seq data with DESeq2. *Genome biology* **15,** 550; 10.1186/s13059-014-0550-8 (2014).

45. Kim, D., Paggi, J. M., Park, C., Bennett, C. & Salzberg, S. L. Graph-based genome alignment and genotyping with HISAT2 and HISAT-genotype. *Nature biotechnology* **37,** 907–915; 10.1038/s41587-019-0201-4 (2019).

46. Hahne, F. & Ivanek, R. Visualizing Genomic Data Using Gviz and Bioconductor. *Methods in molecular biology (Clifton, N.J.)* **1418,** 335–351; 10.1007/978-1-4939-3578-9_16 (2016).

47. Lee, S. *et al.* Comparison between surrogate indexes of insulin sensitivity and resistance and hyperinsulinemic euglycemic clamp estimates in mice. *American journal of physiology. Endocrinology and metabolism* **294,** E261-70; 10.1152/ajpendo.00676.2007 (2008).

48. Geerling, J. J. *et al.* Metformin lowers plasma triglycerides by promoting VLDL-triglyceride clearance by brown adipose tissue in mice. *Diabetes* **63,** 880–891; 10.2337/db13-0194 (2014).

Figures and Figure legends

Figure 1

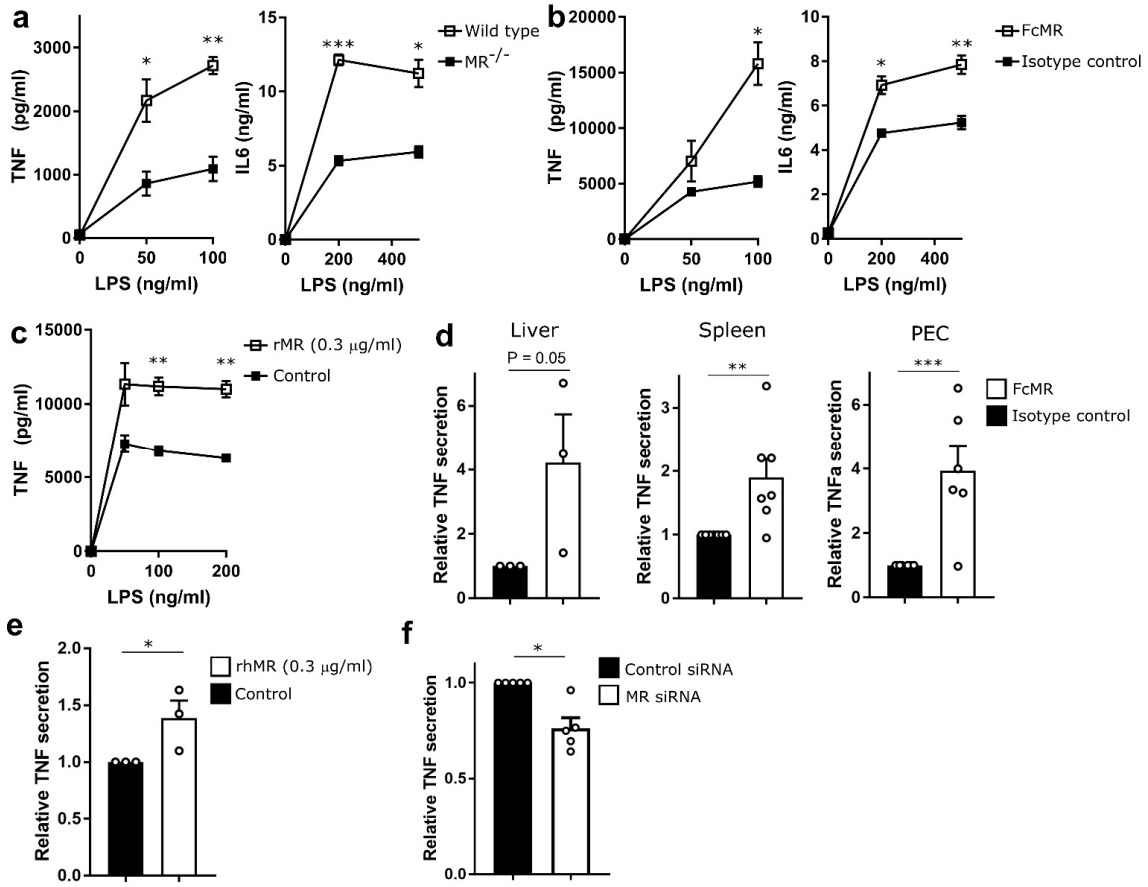

Figure 1: sMR induces pro-inflammatory cytokine secretion by macrophages

a) Secretion of TNF and IL-6 by LPS-treated wild-type or MR-deficient macrophages. b) TNF and IL-6 secretion of LPS-treated MR-deficient macrophages after incubation with FcMR. c) Secretion of TNF by LPS-stimulated MR-deficient macrophages after addition of recombinant MR (rMR). d) Primary murine macrophages were isolated from liver, spleen or peritoneal cavity (PEC) by magnetic separation of F4/80^{+} cells. Secretion of TNF after LPS treatment and stimulation with FcMR were determined by ELISA. e) Secretion of TNF by LPS-treated human monocyte-derived macrophages after stimulation with recombinant human MR (rhMR). f) Secretion of TNF by LPS-stimulated human monocyte-derived macrophages after siRNA-

mediated down-regulation of the MR. All graphs are depicted as mean ± SEM; for all experiments, $n \geq 3$.

Figure 2

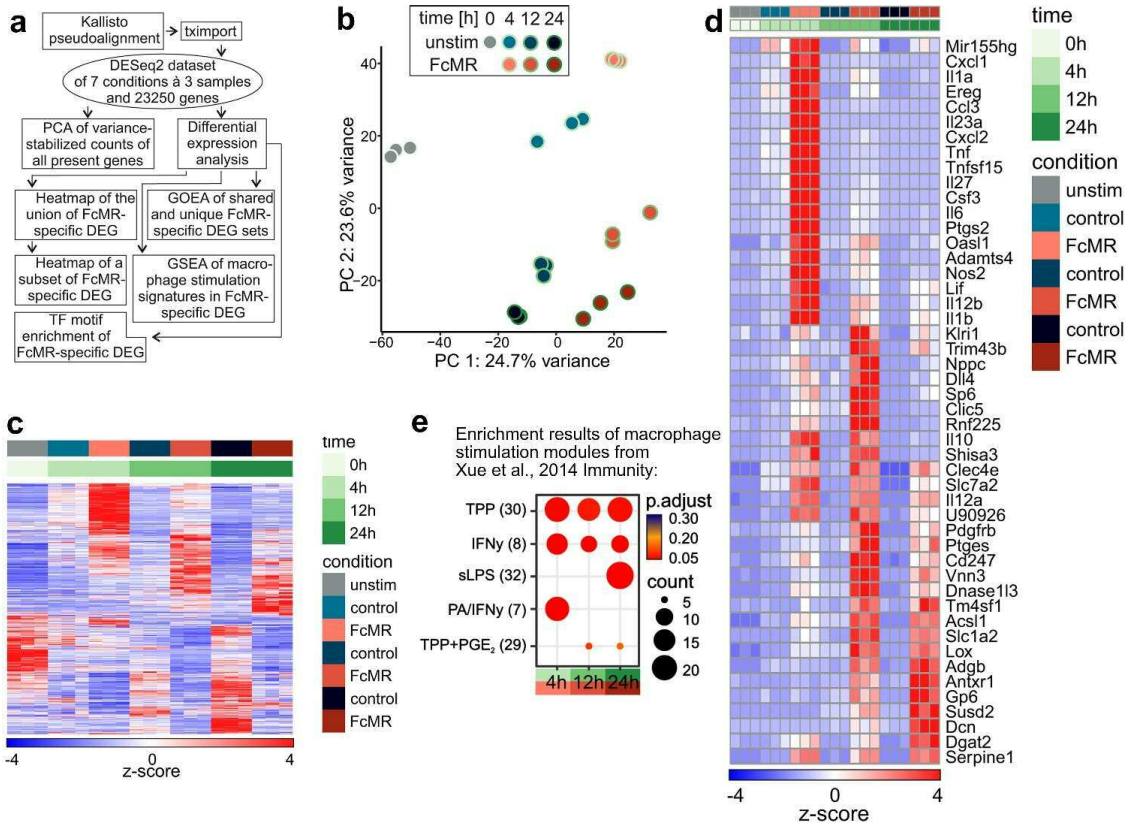

Figure 2: RNAseq analysis of MR-treated macrophages

a) Schematic overview of the bioinformatics RNA-seq analysis strategy. b) Principle component analysis based on variance-stabilized counts of all 23250 present genes. c) Heatmap of hierarchically clustered, normalized and z-scaled expression values of the union of 1366 DE genes between FcMR-treated and control samples. d) Normalized and z-scaled expression values of the union of the top 25 DE genes of each time point significantly upregulated in at least two consecutive time points ranked according to their FcMR vs control samples visualized in a heatmap. e) Dot plot of gene set enrichment analysis results of 49 pre-defined stimulus-specific macrophage expression signatures comprising 28 different stimuli on the FcMR-specific DE genes for each time point. TPP: TNF, PGE2, and Pam3Cys; PA: palmitic acid.

Figure 3

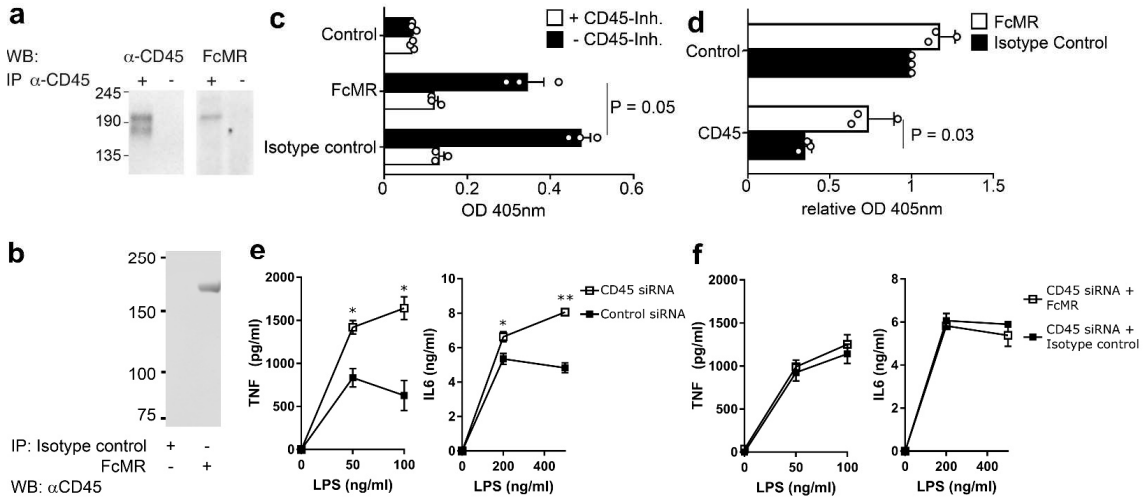

Figure 3: MR inhibits phosphatase activity of CD45 on macrophages

a) Macrophage cell lysates were immune precipitated using a CD45-specific antibody and stained for FcMR binding by far Western Blot. b) Macrophage lysates were immune precipitated with FcMR and stained for CD45 by Western Blot. c) CD45 was precipitated from lysates of FcMR- or isotype control-treated macrophages and incubated with 4-NPP in the presence or absence of the CD45 inhibitor SF1670. Graph depicts CD45-mediated dephosphorylation of 4-NPP measured by colorimetry. Samples without CD45 antibody were used as controls. d) CD45 was precipitated from lysates of FcMR- or isotype control-treated macrophages and incubated with the CD45 substrate TATEGQ-pY-QPQ. Graph depicts the phosphorylation status of TATEGQ-pY-QPQ. Samples without CD45 antibody were used as controls. e) Secretion of TNF and IL-6 by LPS-stimulated macrophages after siRNA-mediated down-regulation of CD45. f) Influence of FcMR on secretion of TNF and IL-6 by LPS-stimulated macrophages after siRNA-mediated down-regulation of CD45. All graphs are depicted as mean ± SEM; for all experiments, $n \geq 3$.

Figure 4

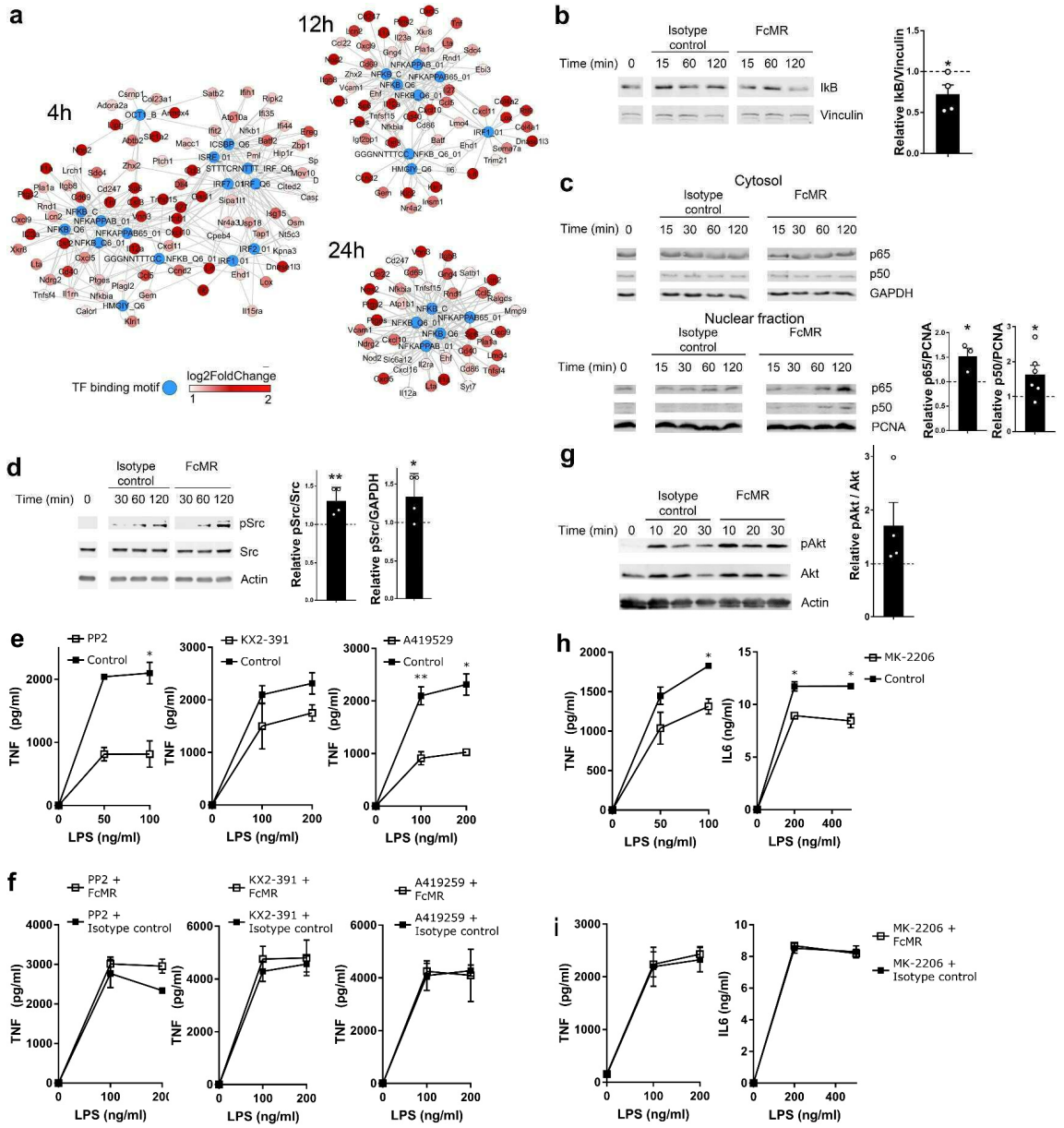

Figure 4: MR reprograms macrophages to a pro-inflammatory phenotype via Src/Akt/NF-κB signaling

a) Network visualization of significantly enriched (q-value < 0.1) TF binding motifs (blue) of the MSigDB motif gene set and potential targets (in red according to their FC) among the upregulated DE genes after 4 h, 12 h or 24 h of FcMR treatment. b) MR-deficient macrophages

were treated with FcMR or isotype control for 60 min. Total IκB was determined by Western Blot. c) MR-deficient macrophages were treated with FcMR or isotype control for 60 min. p65 and p50 were monitored in the cytosolic and nuclear fraction by Western Blot. d) MR-deficient macrophages were treated with FcMR or isotype control for 60 min. Src and phosphorylated Src (pSrc) were determined by Western Blot. e) MR-deficient macrophages were treated with 3 μM PP2, 1 μM KX2-391 or 1 μM A419529 and stimulated with LPS. TNF secretion was monitored by ELISA. f) FcMR-treated MR-deficient macrophages were incubated with PP2, KX2-391 or A419259 and stimulated with LPS. Secretion of TNF was determined by ELISA. g) MR-deficient macrophages were treated with FcMR or isotype control for 30 min. Akt and phosphorylated Akt (pAkt) were determined by Western Blot. h) MR-deficient macrophages were treated with 5 μM MK-2206 and stimulated with LPS. TNF secretion was monitored by ELISA. i) FcMR-treated MR-deficient macrophages were incubated with MK-2206 and stimulated with LPS. Secretion of TNF was determined by ELISA. Graphs are depicted as mean ± SEM; for all experiments, $n \geq 3$.

Figure 5

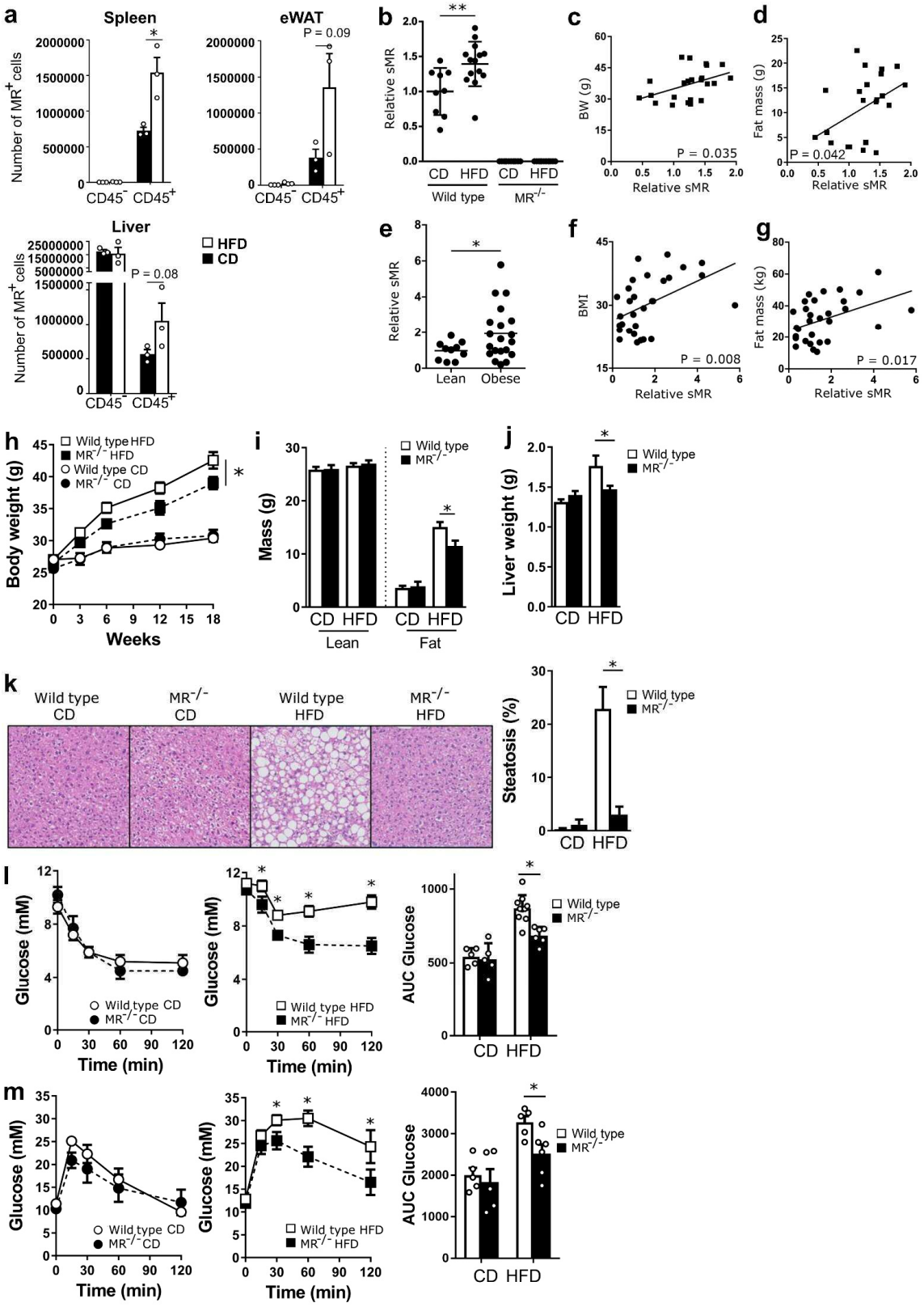
a
Spleen
eWAT
Liver
Number of MR+ cells
CD45- CD45+
P = 0.09
P = 0.08
HFD
CD
b
Relative sMR
CD HFD CD HFD
Wild type
MR-/-
c
BW (g)
P = 0.035
Relative sMR
d
Fat mass (g)
P = 0.042
Relative sMR
e
Relative sMR
Lean Obese
f
BMI
P = 0.008
Relative sMR
g
Fat mass (kg)
P = 0.017
Relative sMR
h
Wild type HFD
MR-/- HFD
Wild type CD
MR-/- CD
Body weight (g)
Weeks
i
Wild type
MR-/-
Mass (g)
CD HFD CD HFD
Lean
Fat
j
Wild type
MR-/-
Liver weight (g)
CD HFD
k
Wild type CD
MR-/- CD
Wild type HFD
MR-/- HFD
Steatosis (%)
CD HFD
l
Glucose (mM)
Time (min)
Wild type CD
MR-/- CD
Wild type HFD
MR-/- HFD
AUC Glucose
CD HFD
m
Glucose (mM)
Time (min)
Wild type CD
MR-/- CD
Wild type HFD
MR-/- HFD
AUC Glucose
CD HFD

Figure 5: sMR is up-regulated in obesity and regulates HFD-induced metabolic dysfunctions and hepatic steatosis

a) MR expression in different organs after HFD or CD feeding. b) sMR levels in the serum of wild-type or MR-deficient mice after HFD or CD feeding. c-d) Correlation of sMR serum levels and body weight (c) or fat mass (d) of all mice depicted in b). e) sMR levels in the serum of lean and obese humans. f-g) Correlation between sMR serum levels and BMI (f) or fat mass (g). h) Body weight of mice on HFD or CD for 18 weeks. i) Lean and fat mass after 18 weeks of diet determined by MRI. j) Liver weight after 18 weeks of diet. k) H&E staining to monitor steatosis. l) Intraperitoneal insulin tolerance test. Blood glucose levels were measured at the indicated time-points and the AUC of the glucose excursion curve was calculated as a surrogate measure for whole-body insulin resistance. m) Intraperitoneal glucose tolerance test. The AUC of the glucose excursion curve was calculated as a surrogate measure for whole-body glucose tolerance. eWAT, epidydimal white adipose tissue. mWAT, mesenteric WAT. iWAT, inguinal WAT. BAT, intrascapular brown adipose tissue. Results are expressed as means ± SEM; n=3 mice per group for a, n=10-15 mice per group for h-k; n= 5-10 mice per group for l-m.

Figure 6

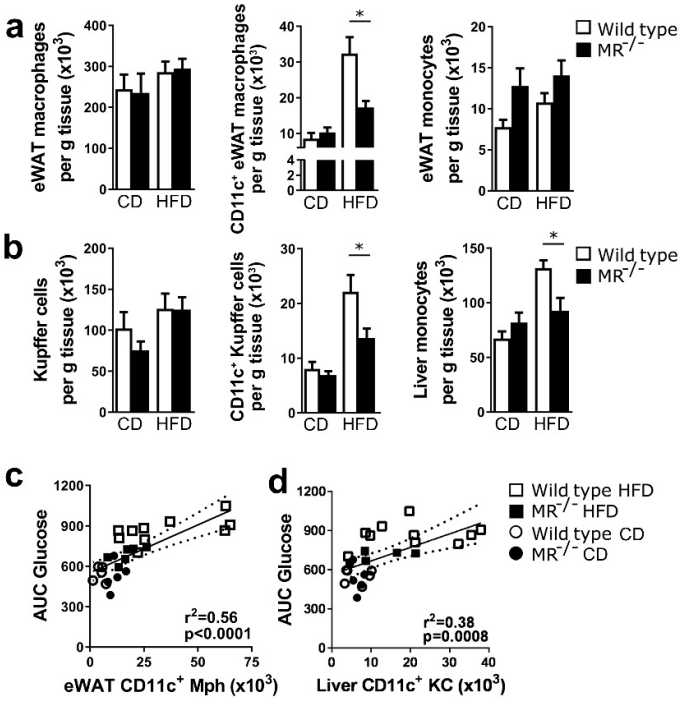

Figure 6: MR regulates WAT and liver macrophage activation after HFD feeding.

a) Numbers of total macrophages, CD11c$^+$ macrophages and monocytes per gram eWAT in HFD- or CD-fed wild-type or MR-deficient mice determined by flow cytometry.b) Numbers of total macrophages, CD11c$^+$ macrophages and monocytes per gram liver in HFD- or CD-fed wild-type or MR-deficient mice determined by flow cytometry. c-d) Correlation between CD11c$^+$ macrophages and whole-body insulin sensitivity, assessed by the area under the curve (AUC) of the glucose excursion curve in eWAT (c) and liver (d). Results are expressed as means ± SEM; n=10-15 mice per group.

Figure 7

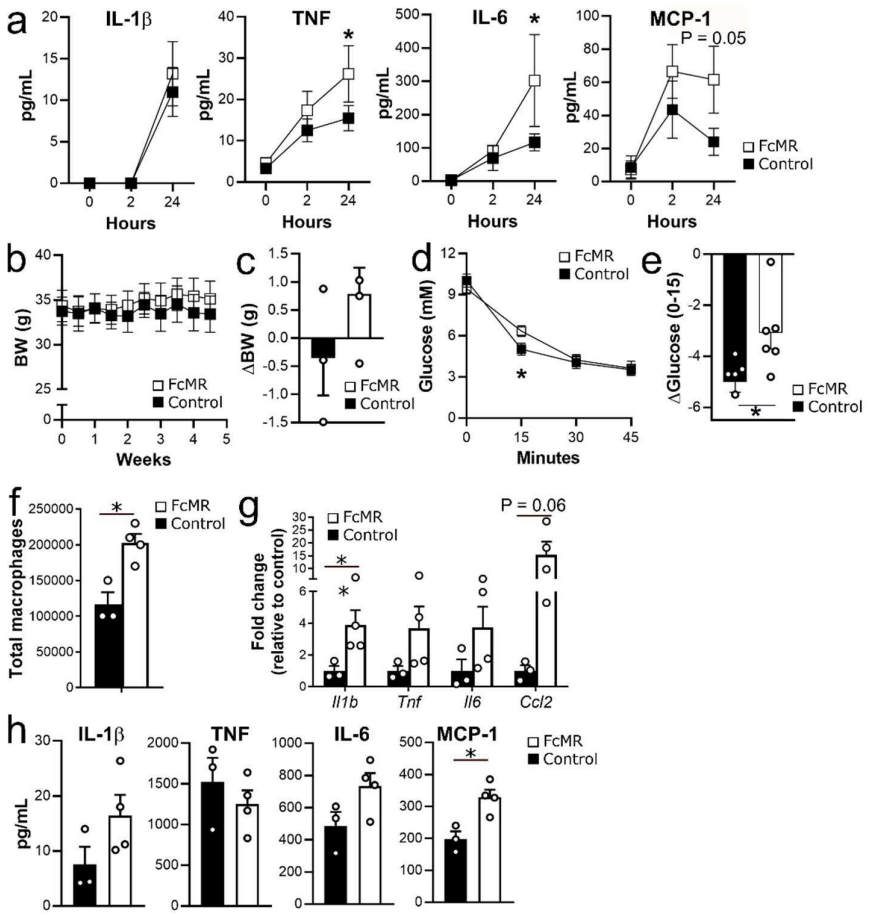

Figure 7: Increased MR levels regulate whole-body metabolism and promote inflammation.

a) CD-fed wild type mice were injected i.p. with 4,82 µmoles/mouse FcMR or isotype control. Serum cytokine concentrations were determined by CBA at the indicated timepoints. b-c) Wild-type mice were fed a CD and concomitantly injected i.p. with 4,82 µmoles/mouse FcMR or isotype control every 3 days. Graphs depict body weight over time (b) and overall change in body weight (c). d-e) Intraperitoneal insulin tolerance test after FcMR treatment of CD-fed mice. Graph in e) shows changes in circulating Glucose levels at 15 min post insulin i.p. f) The number of F4/80^{+} MACS sorted eWAT macrophages was determined after 4 weeks of treatment. g) Expression of inflammatory genes in eWAT was monitored by qPCR. h) Cytokine secretion by F4/80^{+} macrophages from eWAT was determined by CBA after stimulation with

100 ng/ml LPS. BW: body weight. Results are expressed as means ± SEM; n=4-5 mice per group.

Methods

Reagents

α-mouse MR (MR5D3) was from BIO-RAD, α-mouse CD11c (N418), α-mouse panCD45 (30-F11), α–mouse CD45.2 (104), α–mouse CD64 (X54-5/7.1), α-mouse Ly-6C (HK1.4) and α-mouse CD45RA (RA3-6B2) from BioLegend, α-mouse CD45RB (16A), α-mouse CD11c (HL3), α-mouse Siglec-F (E50-2440) and α-mouse CD45RC (DNL-1.9) from BD Biosciences, α-mouse actin (20-33), α-phosphotyrosine (4G10) and α-mouse GAPDH (10B13) from Merck, α-mouse vinculin (4650), α-mouse IκBα (44D4), α-mouse PCNA (PC10), α-mouse Akt (9272), α-mouse pAkt (Ser473)(9271), α-mouse Src (L4A1), α-mouse pSrc (Tyr416)(2101) and α-mouse p65 (D14E12) from Cell Signaling Technology, α-mouse calnexin (ab22595) from Abcam, α-mouse CD11b (M1/70) and α-mouse F4/80 (BM8) from eBiosciences and α-mouse p50 (E10) from Santa Cruz.

Recombinant MR was obtained from R&D Systems, KX2-391 from Biotrend, A-419259 from Biomol, MK-2206 from Enzo Life Sciences, Biotin from Roth, SF1670 from Merck and rhM-CSF from BioLegend. All other chemicals were obtained from Sigma.

Mice and diet

All animal experiments were performed in accordance with the Guide for the Care and Use of Laboratory Animals of the Institute for Laboratory Animal Research and have received approval from the university Ethical Review Boards (DEC No. 12199; Leiden University Medical Center, Leiden, The Netherlands). Male C57BL/6 $MR^{-/-}$ mice and age-matched C57BL/6 wild-type mice from the same breeding facility were housed in a temperature-controlled room with a 12 hour light-dark cycle. Throughout the experiment, food and tap water

were available ad libitum. 8-10 weeks old male mice were randomized according to total body weight, lean and fat mass, and fasting plasma glucose, insulin, TC and TG levels, after which they were fed a high-fat diet (HFD, 45% energy derived from fat, D12451, Research Diets) or a control diet (CD, 10% energy derived from fat, D12450B, Research Diets) for 18 weeks.

For *in vivo* FcMR treatment, C57BL/6 wild-type mice were randomized as above at baseline or after a run-in HFD of 14 weeks. Subsequently, mice were biweekly intraperitoneally injected with 50 µg FcMR or 6.75 µg isotype control, to yield the same administered dose of hIgG1, for four weeks while maintaining the HFD.

Human samples

Serum samples from twenty-six healthy, weight-stable, nonsmoking Caucasian volunteer subjects, 12 lean (2 males, 10 females, BMI 23.3 +/- 0.5 kg/m2) and 14 obese (2 males, 12 females, BMI 35.2 -/- 1.2 kg/m2), this latter before and after weight loss, were collected in the framework of a clinical trial [41] and used to measure circulating sMR in a subset of still available samples. This study (Clinical Trial Registration No. NTR2401) was approved by the Medical Ethics Committee of the Leiden University Medical Centre and performed in accordance with the principles of the revised Declaration of Helsinki. All volunteers gave written informed consent before participation.

Generation of bone marrow-derived macrophages

Bone marrow was flushed from the femurs and tibias of mice and cultured for 7 days in medium containing 2.5 % supernatant of a GM-CSF-producing cell line (total concentration 150 ng/ml).

Generation and purification of FcMR

FcMR proteins (encompassing the CR region, the FN II domain and CTLD1-2 fused to the Fc region of hIgG1) and isotype controls (Fc region of hIgG1) were generated as described previously [10]. For all *in vitro* experiments, FcMR and isotype controls were used in a concentration of 10 µg/ml.

Purification of sMR from the supernatant of MR-expressing cells

Supernatant of bone marrow-derived macrophages was collected and loaded on an affinity chromatography column containing Sepharose beads that were covalently linked to an anti-MR antibody (MR5D3, BIO-RAD). After extensive washing, sMR was eluted in 0.1 M Glycin (pH 2.5), neutralized with 1 M Tris (pH 9.0) and dialysed against PBS containing 10% PEG for 24 h.

Monitoring secretion of TNF and IL-6

Macrophages were incubated with 10 µg/ml FcMR or isotype control, 300 ng/ml recombinant MR (2535-MM-050, R&D Systems), 30 ng/ml purified sMR, 3 µM PP2, 1 µM KX2-391, 1 µM A419259 or 5 µM MK-2206. After 2 h, LPS was added in the given concentrations. Unless indicated differently, supernatants were collected at 3 h (TNF) or 18 h (IL-6) post LPS stimulation, and secreted cytokine levels were measured by ELISA.

Sample preparation for Western Blot analysis

For whole cell lysates, samples were lysed in 10 mM triethanolamine, 150 mM NaCl, 1 mM $MgCl_2$, 1 mM $CaCl_2$ and 1% Triton X-100. For the extraction of nuclear extracts, cells were lysed first in 50 mM HEPES-KOH, 1 mM EDTA (pH 8.0), 140 mM NaCl, 0.25% Triton X-100, 0.5% Igepal and 10% glycerol and the cytosolic fraction was harvested. Afterwards, pellets were resuspended in 10 mM Tris-HCl (pH 8.0), 1 mM EDTA, 100 mM NaCl, 0.5 mM EGTA, 0.1% Sodium desoxycholic acid and 0.5% sodium N-lauryl sarcosine, sonicated and centrifuged, yielding the nuclear fraction.

Surface biotinylation and co-immunoprecipitation experiments

Bone marrow-derived macrophages were incubated with 0.5 mg/ml biotin for 30 min and washed extensively. Afterwards, cells were lysed and 10 µg/ml FcMR was added for 1 h on ice. Subsequently, FcMR was immunoprecipitated using protein A/G-based affinity chromatography and samples were loaded on an SDS-PAGE for analysis by Western Blot using streptavidin or a CD45-specific antibody. Alternatively, a CD45-specific antibody was added to macrophage lysates and precipitated by protein A/G-based affinity chromatography for subsequent far Western Blot analysis using FcMR.

CD45 phosphatase assay

CD45 was immunoprecipitated from macrophage lysates and incubated with 2 mM pNPP for 18 h at 37 °C in the presence or absence of 1 µM of the CD45-specific inhibitor SF1670. Dephosphorylation of pNPP was quantified by colorimetry at 405 nm. Alternatively, immunoprecipitated CD45 was incubated with 0.25 µg of the biotinylated peptide TATEGQpYQPQ for 18 h at 37 °C in the presence or absence of SF1670. Phosphorylated TATEGQpYQPQ was monitored after affinity chromatography using streptavidin-agarose,

staining with the phosphospecific primary antibody 4G10 (Milipore), a HRP-conjugated secondary antibody and addition of the HRP substrate TMB One (Kementec).

siRNA-mediated down-regulation of CD45

siRNA against CD45 (Mm-Ptprc_6 Flexitube siRNA, Qiagen) or control siRNA (AAAAACAUGCAGAAAUGCUGU; containing a specific sequence of the luciferase gene) were obtained from Qiagen. After five days of culture in GM-CSF-containing medium, cells were electroporated with 4 µg siRNA using a Gene Pulser Xcell Electroporation Systems (Bio-Rad) with two sequential pulses of 1000 V for 0.5 msec each. Cells were incubated for 2 days before subsequent experiments were performed.

Blood monocyte-derived macrophages and siRNA-mediated down-regulation of MR expression

Human $CD14^+$ monocytes were isolated from blood of anonymous healthy volunteers, as described previously [42], and cultured in RPMI 1640 (Invitrogen) supplemented with 10% heat-inactivated FSC, 100 U/ml penicillin, 100 µg/ml streptomycin and 50 ng/mL of recombinant human M-CSF (BioLegend) in plates with NunclonTM Delta Surface coating (Nunc). On day 4 of differentiation, cells were electroporated with either 455 nM anti-*Mrc1* siRNA or 455 nM scrambled siRNA (Dharmacon) using the Neon® transfection system (Invitrogen) using one pulse of 1600V for 20 ms. Cells were incubated for 2 days and next incubated for 24 h with 100 ng/ml LPS and 50 ng/ml IFN-γ. Supernatant was harvested after 24 h for analyses of TNF by ELISA using a commercially available kit (BioLegend).

RNA isolation and RNAseq analysis

RNA of $5x10^6$ bone-marrow derived macrophages treated with FcMR or isotype control for 4 h, 12 h and 24 h was isolated with trizol and miRNeasy micro kit (Qiagen) according to the manufacturer's protocol. RNA quality was assessed by visualization of 28S and 18S band integrity on a Tapestation 2200 (Agilent). 100 ng of RNA was converted into cDNA libraries using the TruSeq RNA library preparation kit v2. Size distribution of cDNA libraries was measured using the Agilent high sensitivity DNA assay on a Tapestation 2200 (Agilent). cDNA libraries were quantified using KAPA Library Quantification Kits (Kapa Biosystems). After cluster generation on a cBot, 75 bp single read sequencing was performed on a HiSeq1500.

Bioinformatic analysis

After base calling and de-multiplexing using CASAVA version 1.8.2 and subsequent quality control using fastQC, the 75 bp single-end reads were pseudoaligned to the mm10-based mouse Gencode reference transcriptome vM16 using kallisto version 0.44.0. Transcript abundance estimations were imported to R and summarized on gene level using tximport [43]. Downstream analyses were performed using DESeq2 [44]. After filtering of lowly expressed genes (rowSums > 10) and variance stabilizing transformation, principle component analysis was performed on all present genes using the prcomp package. Differential expression analysis was performed comparing FcMR-treated samples versus controls for each time point without pre-defined log2 fold change threshold and using independent hypothesis weighting (IHW) as the multiple testing procedure. Genes with an adjusted p-value < 0.05 and a fold change (FC) > 2 were determined as significantly differentially expressed. Normalized and z-scaled expression values of the union of differentially expressed (DE) genes over all three time points were visualized in a heatmap. Gene ontology enrichment analyses were performed on those genes shared between all three DE gene sets (shared), as well as the respective gene sets for each time point (4 h, 12

h and 24 h) and those genes unique for each time point (4h.u, 12 h.u and 24 h.u) using the R package ClusterProfiler and visualized in a dot plot. Based on the differential expression analysis, genes with significant upregulation in at least two consecutive time points were selected and ranked according to their FC at each timepoint. Normalized and z-scaled expression values of the union of the top 25 genes for each comparison were visualized in a heatmap. Furthermore, enrichment analysis on the FcMR-specific DE genes for each time point was performed based on 49 previously defined, stimulus-specific macrophage expression signatures encompassing 28 different immunological stimuli [21], using ClusterProfiler‘s “enricher“ function. Significantly enriched signatures were visualized in a dot plot and normalized and z-scaled expression values of the genes to the enriched signatures were plotted in a heatmap. To identify transcriptional regulators responsible for the FcMR-induced changes in gene expression, transcription factor motif enrichment analyses was performed using ClusterProfiler‘s “enricher“ function based on the MSigDB motif gene sets on the FcMR-specific DE genes for each time point. Motifs with q-value < 0.1 were selected and results were visualized in networks showing the enriched TF motifs and their potential targets among the DE genes of the respective comparison using Cytoscape v3.4.0. For determination of the *Cd45* transcript variant expressed in the cells of this data set, reads were aligned to the reference genome mm10 using Hisat2 v2.1.0 [45] and visualized using the R package Gviz [46].

Plasma analysis

Blood samples were collected from the tail tip of 4 h-fasted mice using chilled paraoxon-coated capillaries. sMR serum levels were determined after immune precipitation using a MR-specific antibody, followed by fluorimetry. Blood glucose levels were determined using a Glucometer (Accu-Check, Roche Diagnostics). Plasma total cholesterol (TC; Instruchemie), triglycerides (TG; Instruchemie) and insulin (Chrystal Chem) were determined using commercially available

kits according to the manufacturer's instructions. The homeostatic model assessment of insulin resistance (HOMA-IR) adapted to mice was calculated as ([glucose (mg/dl)*0.055] × [insulin (ng/ml) × 172.1])/3857 and used as a surrogate measure of whole-body insulin resistance [47]. Plasma alanine aminotransferase (ALAT) was measured using a Reflotron® kit (Roche diagnostics).

Insulin and glucose tolerance tests

Body composition was measured by MRI using an EchoMRI (Echo Medical Systems). Whole-body insulin sensitivity was assessed after the indicated time on CD or HFD in 4 h fasted mice by an i.p. insulin tolerance test (ipITT). After an initial blood collection (t=0), an i.p. bolus of insulin (1 U/kg lean body mass; NOVORAPID, Novo Nordisk) was administered to the mice. Blood glucose was measured by tail bleeding at 15, 30, 60, and 120 min after insulin administration using a Glucometer. Whole-body glucose tolerance was assessed after the indicated time on CD or HFD in 6 h fasted mice by an intraperitoneal glucose tolerance test (ipGTT). After an initial blood collection (t=0), an i.p. injection of glucose (2g D-Glucose/kg total body weight, Sigma-Aldrich) was administered in conscious mice. Blood glucose was measured by tail bleeding at 15, 30, 60 and 120 min after glucose administration using a Glucometer (Accu-Check, Roche Diagnostics). At 15 minutes, blood was also collected for analysis of plasma insulin levels as described above.

Histological analyses

A piece of liver (~30 mg) was fixed in 4% paraformaldehyde (PFA; Sigma-Aldrich), paraffin-embedded, sectioned at 4 µm and stained with Hematoxylin and Eosin (H&E). Six fields at 20x magnification (total area 1.68 mm^2) were used for the analysis of hepatic steatosis.

Hepatic lipid composition

Liver lipids were extracted as previously described [48]. Briefly, liver samples (~50 mg) were homogenized in ice-cold methanol. After centrifugation, lipids were extracted with $CH_3OH:CHCl_3$ (1:3 v/v), followed by phase separation with centrifugation (13,000 x g; 15 min at RT). The organic phase was dried and dissolved in 2% Triton X-100 in water. Triglycerides (TG), total cholesterol (TC) and phospholipids (PL) concentrations were measured using commercial kits (Roche Molecular Biochemicals). Liver lipids were expressed as nanomoles per mg protein, which was determined using the Bradford protein assay kit (Sigma-Aldrich).

RNA purification and qRT-PCR

RNA was extracted from snap-frozen tissue samples using Tripure RNA Isolation reagent (Roche Diagnostics). Total RNA (1 µg) was reverse transcribed and quantitative real-time PCR was next performed with the SYBR Green Core Kit on a MyIQ thermal cycler (Bio-Rad). mRNA expression was normalized to *Rplp0* mRNA content and expressed as fold change compared to wild-type CD-fed mice using the ΔΔCT method. Primers were TCAGCCAGATGCAGTTAACGCCC-3′ and 5′-GCTTCTTTGGGACACCTGCTGCT-3′ (Ccl2), GTCCCCAAAGGGATGAGAAG-3′ and 5′-CACTTGGTGGTTTGCTACGA-3′ (Tnf), TGTGCAATGGCAATTCTGAT-3′ and 5′-CTCTGAAGGACTCTGGCTTTG-3′ (Il6), GACCCCAAAAGATGAAGGGCT-3′ and 5′-ATGTGCTGCTGCGAGATTTG-3′ (Il1b), 5′-GCCACCAACCCTTCCTGGCTG-3′ and 5′-TTGGACACTCCTGCTGTGCAGTTG-3′ (Itgax).

Isolation of stromal vascular fraction from adipose tissue

Epididymal adipose tissues were collected in PBS, then minced and digested for 1 h at 37°C in HEPES-buffered Krebs solution (pH 7.4) containing 0.5 mg/mL collagenase type I from *Clostridium histolyticum* (Sigma-Aldrich), 2% (w/v) bovine serum albumin (BSA, fraction V, Sigma-Aldrich) and 6 mM glucose. Disaggregated adipose tissues were passed through 100 µm cell strainers or 200 µm filters and washed with PBS supplemented with 2.5 mM EDTA and 5% FCS. Filtrate was either directly centrifuged (350 x *g*, 10 min at RT) or rested for 10 minutes, after which infranatant was collected and centrifuged. After centrifugation, the supernatant was discarded and the pellet containing the stromal vascular fraction (SVF) was treated with erythrocyte lysis buffer (BD Biosciences). After washing and manual counting, cells were stained with the live/dead marker Aqua or Zombie-UV (Invitrogen), fixed with 1.9% paraformaldehyde (Sigma-Aldrich) and stored in FACS buffer (PBS, 2 mM EDTA, 0.5% BSA [w/v]) at 4 °C in the dark until subsequent analysis performed within 4 days.

Isolation of leukocytes from liver tissue

Livers were collected in ice-cold RPMI 1640 + Glutamax (Life Technologies), minced and digested for 45 min at 37 °C in RPMI 1640 + Glutamax supplemented with 1 mg/mL collagenase type IV from *Clostridium histolyticum*, 2000 U/mL DNase (both Sigma-Aldrich) and 1 mM $CaCl_2$. The digested tissues were next passed through 100 µm cell strainers and washed with PBS/EDTA/FCS. Following centrifugation (530 x g, 10 min at 4 °C), the cell pellet was resuspended in PBS/EDTA/FCS and centrifuged at 50 x g to pellet hepatocytes (3 minutes at 4 °C). The supernatant was next collected and pelleted (530 x g, 10 min at 4 °C), followed by treatment with erythrocyte lysis buffer. After washing, either macrophages or total leukocytes were isolated using LS columns and F4/80 or CD45 MicroBeads (35 µl beads per liver; Miltenyi Biotec), respectively, according to the manufacturer's protocol. Isolated $CD45^+$

cells were counted and processed for flow cytometry as for SVF, and F4/80^{+} cells were stimulated with FcMR and LPS as described above.

Isolation of peritoneal macrophages

Peritoneal wash was collected in PBS supplemented with 2 mM EDTA and centrifuged (530 x g, 10 min at 4 °C). Cell pellet was treated with erythrocyte lysis buffer, counted and processed for flow cytometry as for SVF, or macrophages were isolated using MS columns and F4/80 microbeads according to the manufacturer's protocol.

Isolation of splenic macrophages

Spleens were collected in ice-cold RPMI 1640 + Glutamax, minced and digested for 20 min at 37 °C in RPMI 1640 + Glutamax supplemented with 1 mg/mL collagenase D (Sigma) and 2000 U/mL DNase. The digested tissues were next passed through 100 µm cell strainers and washed with PBS/EDTA/FCS. Following centrifugation (530 x g, 10 min at 4 °C), the cell pellet was treated with erythrocyte lysis buffer. Cells were either counted and processed for flow cytometry as for SVF, or macrophages were isolated using MS columns and F4/80 microbeads according to the manufacturer's protocol.

Flow cytometry of WAT and liver myeloid subsets

Part of the cells were first permeabilized with 0.5% saponin (Sigma-Aldrich) or eBioscience permeabilization buffer (Invitrogen). After washing, cells were next stained with antibodies directed against CD45, CD45RA, CD45RB, CD45RC, CD45.2, CD64 , Siglec-F , CD11b,

Ly6C, F4/80 and CD11c in permeabilization buffer. Cells were measured on a FACSCanto flow cytometer or LSR-II (both BD Biosciences), and gates were set according to Fluorescence Minus One (FMO) controls.

Quantification and statistical analysis

All *in vivo* data were analyzed by two-way ANOVA with multiple comparisons followed by post-hoc Fisher's LSD test. For all other experiments, P values and statistical significance was calculated by a two-sided student´s t-test. Single data points represent mean values of distinct independent experiments for all *in vitro* experiments. For all *in vitro* experiments, single data points represent individual mice. * $P<0.05$; ** $P<0.01$ and *** $P<0.001$. All graphs depict mean value ± SEM of at least three independent experiments.

Data and Software availability

The complete RNAseq analysis incl. code and count data can be found under jsschrepping/Embgenbroich_2020 at https://github.com/schultzelab. Additionally, the unprocessed RNA-seq data is available online in the Gene Expression Omnibus (GEO) database (https://www.ncbi.nlm.nih.gov) under accession number GSE145369.